UNIVERSITÀ DI PARMA
ARCHIVIO DELLA RICERCA

University of Parma Research Repository

Laser milling of martensitic stainless steels using spiral trajectories

This is a pre print version of the following article:

Original
Laser milling of martensitic stainless steels using spiral trajectories / Romoli, Luca; Tantussi, F.; Fuso, F.. - In: OPTICS AND LASERS IN ENGINEERING. - ISSN 0143-8166. - 91:(2017), pp. 160-168. [10.1016/j.optlaseng.2016.11.016]

Availability:
This version is available at: 11381/2824535 since: 2021-10-18T10:29:12Z

Publisher:
Elsevier Ltd

Published
DOI:10.1016/j.optlaseng.2016.11.016

Terms of use:

Anyone can freely access the full text of works made available as "Open Access". Works made available

Publisher copyright

note finali coverpage

(Article begins on next page)

08 December 2025

Manuscript Details

Manuscript number	OLEN_2016_25
Title	Laser milling of martensitic stainless steels using spiral trajectories
Article type	Full Length Article

Abstract

A laser beam with sub-picosecond pulse duration was driven in spiral trajectories to perform micro-milling of martensitic stainless steel. The geometry of the machined micro-grooves channels was investigated by a specifically conceived Scanning Probe Microscopy instrument and linked to laser parameters by using an experimental approach combining the beam energy distribution profile and the absorption phenomena in the material. Preliminary analysis shows that, despite the numerous parameters involved in the process, layer removal obtained by spiral trajectories, varying the radial overlap, allows for a controllable depth of cut combined to a flattening effect of surface roughness. Combining the developed machining strategy to a feed motion of the work stage, could represent a method to obtain three-dimensional structures with a resolution of few microns, with an areal roughness Sa below 100 nm.

Keywords	Laser; Micro machining; Stainless steel; Roughness

Corresponding Author	Luca Romoli
Order of Authors	Luca Romoli, Francesco Tantussi, Francesco Fuso

Suggested reviewers	Olga Varlamova, Blunt Liam, Marc Faucon, Mohammad Muhshin Aziz Khan

Submission Files Included in this PDF

File Name [File Type]

Cover letter_OLEN2016.doc [Cover Letter]

man_rev_21_sett_f.doc [Manuscript File]

highlights.doc [Highlights]

To view all the submission files, including those not included in the PDF, click on the manuscript title on your EVISE Homepage, then click 'Download zip file'.

UNIVERSITY OF PARMA
IED - Industrial Engineering Department
Parco Area delle Scienze 181/A, 43124 Parma - Italy

Parma, 27 September 2016

To: **Prof. Pramod K. Rastogi**
Editor-in-Chief, Optics and Lasers in Engineering

Subject: Submission of a new manuscript

Dear Sir,

attached is the article entitled "LASER MILLING OF MARTENSITIC STAINLESS STEELS USING SPIRAL TRAJECTORIES" which, I hope, will be accepted as a candidate for publication to your valued journal.

I affirm that the manuscript has been prepared in accordance with Instructions to Authors. I have read the manuscript and I hereby affirm that the content of this manuscript or a major portion thereof has not been published in a refereed journal, and it is not being submitted for publication elsewhere.

Thank you very much.

Sincerely yours
Dr. Luca Romoli

Complete address : Prof. Luca Romoli, PhD
Università di Parma
Dipartimento di Ingegneria Industriale
Parco Area delle Scienze 181/A
43124 PARMA - ITALY
phone: (+39)-0521-906202 (direct)
e-mail: luca.romoli@unipr.it

Contents lists available at SciVerse ScienceDirect

Optics and Lasers in Engineering

Journal homepage:

Laser milling of martensitic stainless steels using spiral trajectories

L. Romoli[1], F. Tantussi[2], F. Fuso[3,4]

[1] Department of Industrial Engineering, University of Parma, Italy
[2] Istituto Italiano di Tecnologia, Italy
[3] Department of Physics "Enrico Fermi" and CNISM, University of Pisa, Italy
[4] INO-CNR, Pisa, Italy

A laser beam with sub-picosecond pulse duration was driven in spiral trajectories to perform micro-milling of martensitic stainless steel. The geometry of the machined micro-grooves channels was investigated by a specifically conceived Scanning Probe Microscopy instrument and linked to laser parameters by using an experimental approach combining the beam energy distribution profile and the absorption phenomena in the material. Preliminary analysis shows that, despite the numerous parameters involved in the process, layer removal obtained by spiral trajectories, varying the radial overlap, allows for a controllable depth of cut combined to a flattening effect of surface roughness. Combining the developed machining strategy to a feed motion of the work stage, could represent a method to obtain three-dimensional structures with a resolution of few microns, with an areal roughness S_a below 100 nm.

Keywords: Laser, Micro machining, Stainless steel, Roughness

1. Introduction

The increasing concern for the micro-fabrication of moulds, sensors, actuators, micro optics, micro-fluidic components and other micro-system devices, has pushed companies towards innovative and versatile machining methods. Among all, laser milling has demonstrated to be a flexible process suitable for machining difficult-to-machine materials like ceramics, dielectrics, carbide and hardened steel with high productivity and surface quality. Compared with other conventional mechanical processes, laser micro-machining is a non-contact material removal process that removes much less material, involves highly localized heat input to the workpiece, minimizes distortion, and offers no tool wear. Therefore, the process is not limited by constraints such as maximum tool force, build up edge formation, or tool chatter [1].

In laser milling a focused laser beam is scanned over the workpiece, removing material layer by layer. As for conventional milling, the scanning pattern can be different for each layer, and as a result this 2.5D machining method can produce 3D shaped surface structures [2]. The key-factor of such a process resides mainly in the control of the ablation depth per layer [3]. This parameter represents the thickness of the single removed layer irradiated by the laser and it is opposed to the surface roughness in the definition of the process robustness. The ablation depth, and consequently the surface roughness, are determined by the laser beam characteristics (wavelength, pulse duration, peak power, repetition rate), by the strategy on which the surface is irradiated (scan speed, scan strategy per layer) and obviously by the chemistry and physical properties of the workpiece.

The trade-off between productivity and surface quality (e.g. roughness, burrs, melt deposits, etc.) is frequently argued in the literature. Representative examples can be found in [4] where the performance of micromilling of AISI H13 can be obtained as a balance between the conditions for minimum surface roughness and maximum ablation depth. Multi-objective process parameters optimization is also a frequent tool used to perform a statistical optimization of laser micromilling: in [5] it was used to enhance the ablation capability of T-shaped features on tool steels while in [6] it was adopted to derive the best set of process parameters for the micromilling of aluminium 5754.

A possible way to mitigate such a trade-off resides in shortening the laser pulse duration below the characteristic time for which the pulse energy is transformed into heat on the workpiece. The combination of pulse peak power and pulse duration significantly influences the material removal mechanism: for long pulses (micro- and nano-second) and peak power density ranging between 10^9-10^{11} W/cm^2, the material is removed by melt expulsion, combining material vaporization and melting. Those sources show high production rates against low quality generated by melt accretions and thermal damage of the workpiece [7]. Due to the large amount of melt ejection and spatter formation involved in the process, the quality and reproducibility of the micromilled cavity is rather low [8]. If higher precision is needed, short and ultrashort laser pulses have to be applied. According to [9], a pulse is ultrashort when the diffusion depth during the pulse is in the same order or smaller than the skin layer depth in the Beer-Lambert absorption law. With ultrashort laser pulses and high power density (above 10^9 W/cm^2) the material is removed with minimized heat impact: the laser interacts with the material in the solid state only, and direct solid-vapour transition occurs. In case of metals, 1 ps can be retained a threshold value for transition from short to ultrashort [7]. As a result, no heat related defects occur – e.g., no burrs, thermal stress, melt, chipping, or cracking – and very thin substrates can be processed without breaking or deformation. The small ablation rate (tens of μm^3 per pulse) can be significantly increased using repetition rate in the order of 100 kHz or even higher, as reported in [10]. Using high repetition rates is also beneficial in terms of surface roughness since a much higher pulse overlap can be obtained at scan speeds of several meters per second. A more uniform removal over the scanned beam trajectory avoids an alternation of peak and valley which strongly lowers surface quality [11].

A second possible alternative to increase the surface quality concerns the scan strategy per layer: being an intensified source of energy, the laser beam is used as a sharp-edged tool which

produces grooves to be flanked and partially superimposed to determine the removal of a layer. The surface roughness can be then predicted by knowing the spacing between the groove, also defined as hatch distance parameter and the ablated depth per groove (which is in turn function of process parameters) [12]. More complex but semi-empirical models have been proposed in [13] for the laser milling of PMMA obtained by flanking parallel grooves of Gaussian profile.

A similar strategy of layer removal was used in laser micro-turning [14]: also in this case the surface roughness is determined by flanking of surface peaks and valleys generated by superimposed grooves along the spiral trajectory of the beam on the cylindrical surface of the specimen. Average values of R_a were found in the range of 2-6 µm, corresponding to a finishing procedure in conventional machining with chip removal.

The literature testifies that despite the already existing applications of ultrashort pulse laser milling (e.g. the shaping of micro moulds [15] and micro cutting tools [16], machining of complex lab-on-a-chip structures [17]) the topic of the surface finishing obtainable at the bottom of the removed layer is still a main concern for a machining technique which should enable the high accuracy to fulfil the requirements of precision engineering.

The accuracy obtainable on the working plane is typically in the micrometer range and it depends on the positioning stages but also on the optics adopted. On the other hand, the accuracy and the surface quality in the depth direction depend not only on the process settings, but also on the composition and finish of the material used. The best results are usually obtained with a fine grain or amorphous material structure and a polished surface to begin with. Therefore the first objective of the present research is to investigate the laser micro-milling process in real industrial conditions performing experiments using a production fs-laser source and stainless-steel samples in as-delivered conditions. This will allow to determine if the initial surface roughness, which has almost the same scale of the removal depth per layer, influences the material removal and the formation of the new surface topography.

With the objective of increasing the surface quality with respect to the available literature, a new set-up was established in this study to perform laser micro-milling. The engraving strategy can be pinpointed as follows:

- the laser beam was firstly moved along circular trajectories varying process parameters in order to define the cross profile of each groove (depth and width) as a preliminary step in determining the ablation depth;
- Once the groove profile was established, the beam was then moved in spiral trajectories to perform the removal of a layer. The radial overlap was varied and the obtained surface investigated, in view of the removal of circular pockets.
- Laser parameters and scanning strategies were studied in order to ascertain their role in determining a controllable ablation depth per layer and a surface roughness lower than that available in the literature for similar processes.
- Final ambition of the present article is to give fundamentals for the micro-milling of three-dimensional structures ranging from ten to several hundreds microns with a controlled roughness well below 1 µm.

2. Materials and methods

2.1. Sample preparation

Experiments were carried out on AISI 440C stainless steel, 0.35 mm thick, circular plates with a diameter of 14 mm and an arithmetical mean roughness R_a in the range 0.2-0.3 µm. Plates at as-delivered conditions present an anisotropic roughness due to the final grinding procedure, as highlighted in Fig. 1. The AISI 440 C is a martensitic stainless steel (composition given in Table 1) that presents high resistance to corrosion and to wear, massively used in automotive industry.

Each plate was milled in order to create two planar surfaces used as reference to define the position of the workpiece during the laser processing .

Table 1. Chemical composition of AISI 440C Stainless Steel.

	Element						
	C	Cr	Mn	S	Si	Mo	Se
Composition in wt.%	0.95-1.2	17.2	1.00	0.015	1.0	0.75	0.20

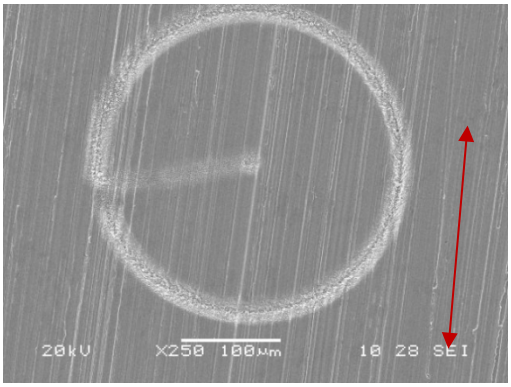

Fig. 1. SEM micrograph of a laser-machined sample. Red arrows highlight the anisotropic roughness due to mechanical machining.

2.2. Experimental setup

A fibre fs-laser system (Raydiance Starfemto R-100) was used to generate linearly polarized laser pulses with a duration τ = 800 fs, a central wavelength λ = 1552 nm and a maximum pulse energy E_P =50 µJ at a repetition rate f = 100 kHz. The laser source was equipped with a 3D scan head (Arges Precession Elephant) with up to five axes, schematically represented in Fig. 2.

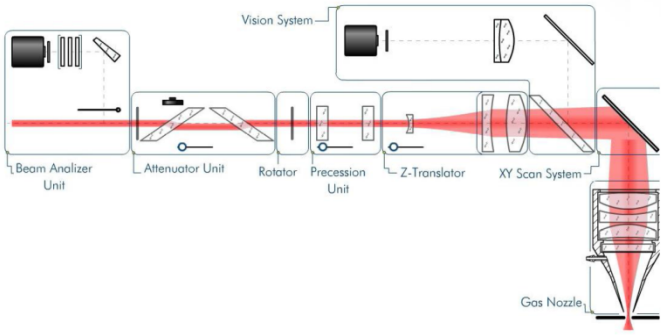

Fig. 2. A schematic representation of the 3D Scan head [18].

The attenuator unit allowed the variation of laser power while the rotator, consisting in a $\lambda/4$ plate, was used to obtain circularly polarized pulses. The angle of incidence can be modified by means of the precession unit with a maximum inclination of about 7° with respect to the ablated surface. The Z-translator was used to adjust the focus distance while the XY scan system consisted in two mirrors mounted onto galvanometers, providing the possibility to draw desired shapes on the workpiece. Therefore, the scan head allowed to realize circular, elliptical, spiral and helicoidal paths with a range of incidence angles.

In the present experimental activities, the raw beam (3.8 mm diameter, M^2=1.2) was circularly polarized and focused on the top surface of the workpiece to a minimum spot size of 20 µm diameter with a nearly Gaussian energy distribution. Pressurized Helium at 5 bar was used as assist gas to shield the incidence of plasma plumes ignited from the metal vapour evolving by the surface.

2.3. Laser processing

Refined laser micro-miling starts from the engraving of single tracks onto the specimen. In order to study the effects of process parameters on the cross-profile (depth and width) of such grooves, the beam was moved along circular trajectories.
Taking into consideration the as-delivered surface roughness, circular grooves with a diameter of 300 µm were performed. This choice allowed to afford the uniformity of the ablation process as well as the formation of surface structures irrespective to the angle between the tangential speed and the roughness direction.
Two main parameters were considered in order to investigate different material removing regimes: the pulse energy and the laser tangential speed. The repetition rate was kept constant at the maximum value of 100 kHz thus ensuring the highest pulse overlap as possible within the range of tangential speed used (from 92% to 98%). Table 2 summarizes levels and values selected for each parameter.
Moreover, three levels of angle of incidence were set in order to investigate the effect of the debris depositions on the edges of the groove and the slope of the groove profile.

Table 2. Levels and values for selected parameters.

	Parameters			
Sample n°	Pulse energy, E_P (µJ)	Tangential speed, v (mm/s)	Angle of incidence, AI (°)	Energy density, ED (J/mm^2)
1	50	25	0	10.0
2	50	50	0	5.0
3	50	75	0	3.3
4	40	25	0	8.0
5	40	50	0	4.0
6	40	75	0	2.6
7	30	25	0	6.0
8	30	50	0	3.0
9	30	75	0	2.0
10	20	25	0	4.0
11	20	50	0	2.0
12	20	75	0	1.3
13	10	25	0	2.0
14	10	50	0	1.0
15	10	75	0	0.6
16	30	25	3	6.0
17	30	25	-3	6.0
18	50	50	3	5.0
19	50	50	-3	5.0

Most of the tests were performed by sending the laser radiation perpendicularly to the specimen surface with an angle of *incidence AI* = 0°. The positive value of the angle of incidence means that the beam was directed towards the outside of the mark while the negative value means that it was directed towards the centre, as represented in Fig. 3.

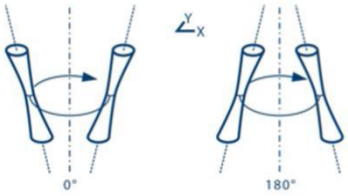

Fig. 3. Angle of incidence: positive (left) and negative (right) values [18].

The last column of table 2 lists the values of Energy Density ED (J/mm^2) calculated according to

$$ED = \frac{E_P \cdot f}{v \cdot \phi_{SPOT}} \quad (1)$$

ED represents a direct relationship between the average laser power (the product of pulse energy E_P and repetition frequency f), the scanning speed v, and the laser spot diameter ϕ_{SPOT}.
A 2x9 array of marks was produced on each plate: each mark consists in a circular path with a diameter of 300 µm. The laser beam started at the centre of the groove, moved linearly for 150 um and finally produced a 360° clockwise circular trajectory. Grooves on the same column have been processed with the same set of parameters in order to evaluate the repeatability of the process. Therefore, nine different sets were processed on each workpiece.

2.4. Characterisation

First, marked surfaces were inspected by Scanning Electron Microscopy (SEM) to reconstruct the surface morphology. SEM was used for qualitative analyses in order to visualize the generated surface textures and to characterize the geometrical features. In fact planar imaging was not suited for direct measurement of the surface roughness.

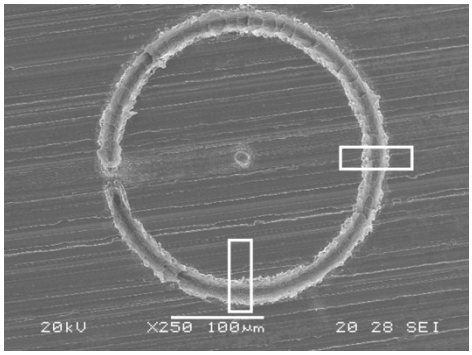

Fig. 4. SEM image of a circular groove with the position of the scan areas.

Second, a Shear Force Microscope (ShFM), tested and tailored to the inspection of high-precision components in a previous research [19], was used to acquire topography maps of the surface.
The sample was mounted on a three-axis closed-loop nanopositioner (Physik-Instrumente PI.517, 3CL) that allowed for a maximum travel of 100 µm in the in-plane (x, y) directions and 20 µm in the vertical (z) direction. The nanopositioner was driven by a controller for scanning probe microscopy (RHK SPM 100).
The scan speed (between 0.10 and 1.00 µm/s) was set depending on the surface profile, taking into consideration the response time

of the feedback controller in order to avoid contacts between the tip and the sample.
The ShFM was used to reconstruct the topography map of the sample as an h(x, y) matrix, obtained while scanning the sample in a raster path. The matrix can be subsequently processed by software, for 2D and 3D maps rendering, line profiles extraction, roughness analysis and evaluation of other surface properties.
Taking into consideration the surface roughness, two rectangular areas placed at a distance of 90 degree along the circular path were scanned, as reported in Fig. 4. The scan direction is then parallel to the roughness primary texture for one area while it is perpendicular for the second one. As it was above anticipated, the results of the analysis testify that the primary texture of the surface did not play any observable role in the features (ablation depth, roughness) of the machined surface.

3. Results and discussion

3.1. Groove profile

Dimensions of the grooves were calculated for each scanned area by extracting profiles as reported in Fig. 5. For each profile a theoretical plane was defined considering the external portions of profile that were not involved by the laser ablation. The aim is to filter from the groove profile eventual deposits of debris and ejected material at the groove edges, as well as any other form of burr. Taking into account the nearly Gaussian profile of the beam and the Beer-Lambert absorption law, the groove profile was evaluated with a parabolic function (see Section 3.2) fitting the acquired data. The groove maximum depth D was calculated as the maximum distance between the parabolic function and the mean plane while the groove width H was calculated as the distance between the intersections of the parabolic function with the mean plane, as shown in Fig. 5.

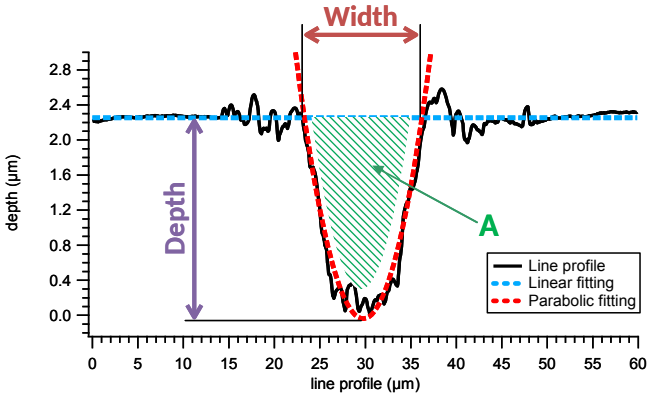

Fig. 5. Evaluation of the dimensions of the mark on a profile

The average depth calculated over four measurements (two different positions for the two different grooves) is reported in Fig. 6 as a function of energy density. Depth was found to increase with energy density with an almost linear trend up to 4 J/mm^2. Beyond this limiting value the use of scanning speed of 75 mm/s resulted in a lower growth rate. Figure 6 points out that the deepest grooves were obviously obtained with the lowest value of tangential speed corresponding to the highest pulse overlap.
The average width values are reported in Fig. 7 as a function of energy density. Width was found to slightly increase with energy density: even with the lowest values of the energy density explored here, widths of about 15 µm were obtained while the limiting value of 20 µm corresponding to the focused beam diameter was reached at about 10 J/mm^2. The tangential speed itself was not found to have a significant impact in determining the groove width.

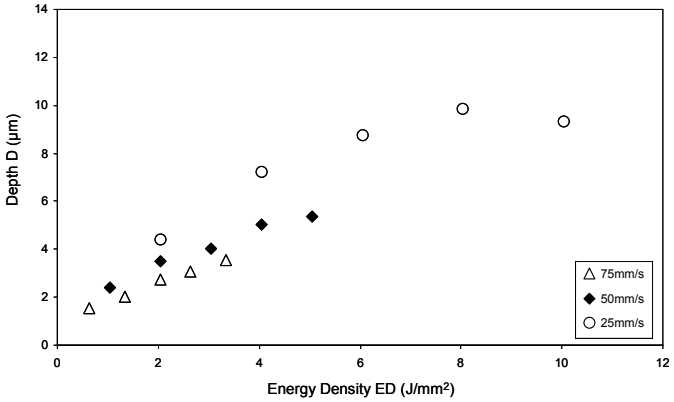

Fig. 6. Groove depth as a function of the ED used.. For the sake of clarity, the error bars accounting for the dispersion of the results obtained in different scans of samples machined in the same conditions are not reported. Their contribution can be estimated below 15% of the plotted values.

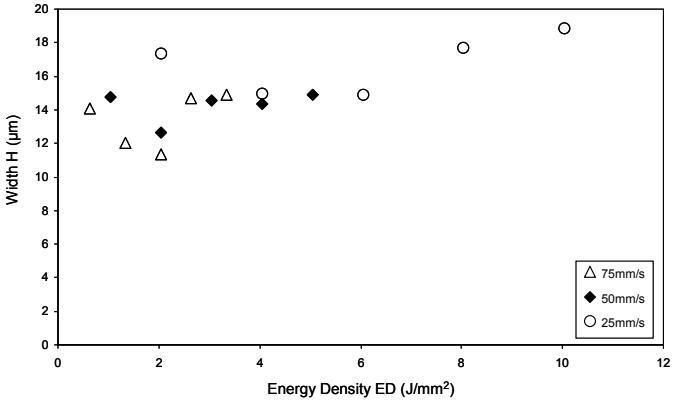

Fig. 7. Groove width as a function of the ED used. For the sake of clarity, the error bars accounting for the dispersion of the results obtained in different scans of samples machined in the same conditions are not reported. Their contribution can be estimated below 15% of the plotted values.

The Material Removal Rate MRR (mm^3/s) was calculated as the product between the tangential speed of the laser beam and the cross section of the groove as reported in eq. (2):

$$MRR = A \cdot v \tag{2}$$

where A is the removed area estimated as the intersection of the mean plane with the parabolic profile of the groove (as reported in Fig. 5) and v is the tangential speed.
The graph in Fig. 8 shows that, accordingly to the trend of the depth, the material removal rate is almost linearly proportional to the energy density used.
The Specific Energy consumption SE (J/mm^3) was calculated in eq. (3) as the ratio between the total energy E_T released by the laser in a volume V of material. SE can also be expressed as the ratio between the average laser power W and the material removal rate

$$SE = \frac{E_T}{V} = \frac{W}{MRR} \tag{3}.$$

Figure 9 shows the trend of the specific energy as a function of the energy density, highlighting the influence of the tangential speed.

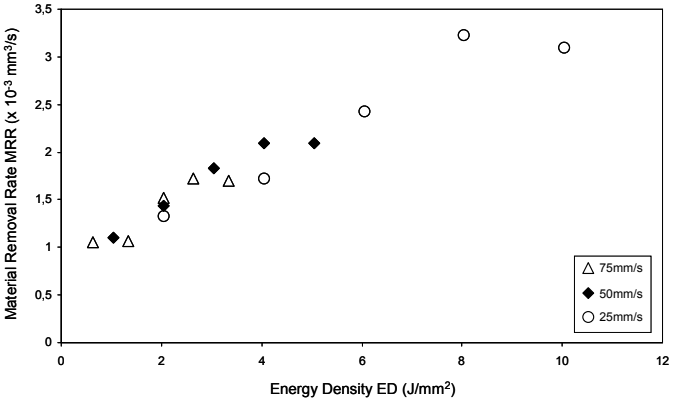

Fig. 8. Material removal rate as a function of the *ED* used.

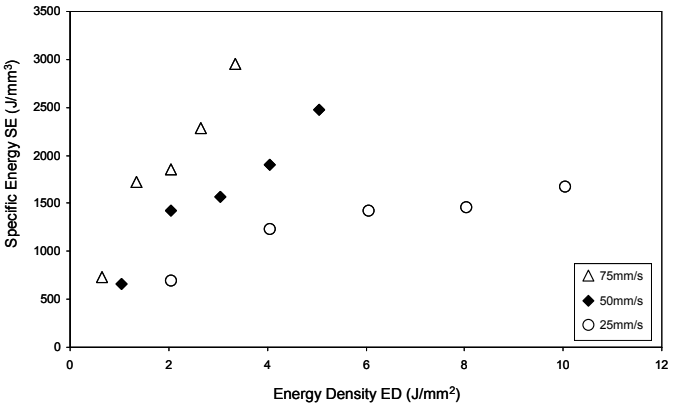

Fig. 9. Specific energy as a function of the *ED* used.

Data reported in the graph show that specific energy is lower for tangential speed of 25 mm/s: the material removal appears to be more effective at the lowest value of the tangential speed. This phenomenon can be explained considering that at low tangential speed the laser beam irradiates a much smaller area in the unit time, removing material more in depth. A deeper groove profile enables to trap an higher percentage of the laser beam energy, reducing the reflectivity of the surface and thus favouring the absorption phenomena.

3.2 Modelling groove profile

In the perspective to use the circular engraving as a preliminary step to laser-mill layers of material, a model to predict the groove profile is here hypothesized based on the experimental data collected. Considering that the laser pulse duration of 800 fs is shorter than the photon-phonon relaxation time (nearly 1 ps for metals) the main assumption of the model is that the energy released by the laser was not converted into heat during the material removal. In agreement with this statement, the fraction of laser power not reflected by the surface is completely made available to the purposes of ablation. Furthermore, the surface reflectivity is supposed to keep a constant value during the ablation process, neglecting any possible modifications of the physical properties of the material during the pulse evolution and any effects related to the variation of the surface roughness eventually occurring pulse after pulse. The energy released by the laser is then fully used for photo-chemical ablation and absorbed in the material according to Gaussian distribution of the energy across the beam in combination with the Beer-Lambert absorption law. The absorbed energy per unit surface *AE* has the following distribution in the material:

$$AE = ED_{MAX} \cdot e^{-\frac{2x^2}{r_0^2}} \cdot e^{-\frac{z}{D_P}} \tag{4}$$

where r_0 is the laser spot radius on the sample surface, D_P the depth where the energy density is reduced by a factor ($1/e$) and ED_{MAX} the maximum value of the energy density (the top value of the beam Gaussian distribution) expressed as a function of the absorbed power of the beam $W(1-r)$, being r the reflectivity of the material and W the average power. Moreover, in case of Gaussian laser beam distribution (TEM0,0), ED_{MAX} can be calculated as follows:

$$ED_{MAX} = \sqrt{\frac{2}{\pi}} \frac{W(1-r)}{r_0 v} \tag{5}$$

where v is the tangential speed of the laser beam. It was here assumed that the material was removed by ablation when the energy density in the workpiece overcame a threshold value of energy ED_C (critical energy). It was then possible to calculate the geometrical profile for which the energy provided by the laser exceeded ED_C. It resulted in a removed parabolic section having width H and depth D:

$$H = 2r_0 \sqrt{\frac{1}{2} \ln \frac{ED_{MAX}}{ED_C}} \tag{6}$$

$$D = D_P \ln \frac{ED_{MAX}}{ED_C} \tag{7}.$$

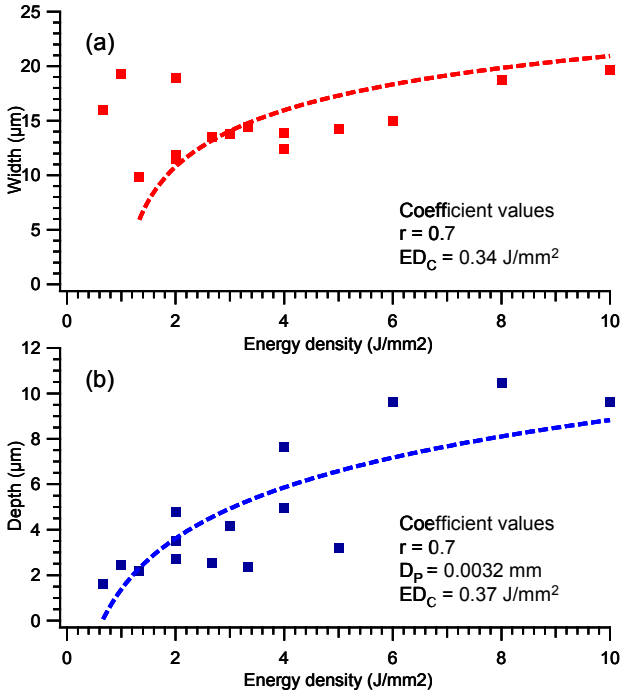

Fig.10. Nonlinear regression of the measured data with respect to the energy density used in the experiments. Panel (a) shows the experimental procedure for the width while panel (b) shows the one for the depth.

Considering the material reflectivity r = 0.7 as reported in [20] the measured data for the groove width were fitted by a nonlinear regression. Panel (a) in Fig. 10 shows that a critical energy ED_C = 0.34 J/mm^2 can be derived for the width. Using the same procedure data measured for the depth were analysed, as in panel (b) in Fig. 10, to derive an absorption depth D_P of about 3.2

μm and a critical energy ED_C = 0.37 J/mm², very close to the value obtained in the analysis of the width data. These values reflect the physics of the ablation process since penetrating the bulk material along the optical axis requires more energy than leaving a track orthogonal to the axis. An average value of the critical energy of 0.35 J/mm² can be assumed for the combination of laser setup and material adopted.
Even though the model includes several simplified assumptions and experimental data do not fully follow the predicted trend, it can be adopted to roughly estimate width and depth of the engraved grooves. This is in turn useful to find the most suitable strategy in view of laser milling of extended areas. A predefined groove profile, at least within the limits of the tested values, is then obtainable by selecting process parameters in accordance to the relationship between energy density and the groove geometrical features expressed in equations 6 and 7.

3.3 Burr formation on channel edges

Inspections with SEM and measurements of the groove profile by ShFM showed the presence of deposits along the groove edges when using energy density higher than 2.5 J/mm². This phenomenon is evident in Fig. 12.

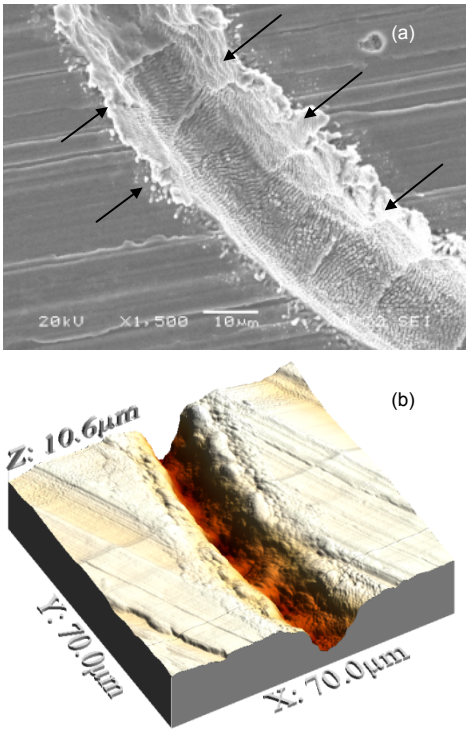

Fig.12. Sample number 10, groove obtained at E_P = 20 μJ, v = 25 mm/s and AI = 0°. Panel (a) shows the SEM detail of the groove with red arrows pointing at the burrs; panel (b) shows the 3D ShFM topography of the groove profile and its surroundings.

The height of those burrs, which are mainly composed by material expelled from the groove, can reach 2-5 μm thus limiting the quality of the milling process.
With the objective to reduce the occurrence of deposition of ejected material along the groove profile, the circular ablation was carried out in a limited number of samples (see table 2) inclining the beam of ±3° which corresponded to 50% of the range allowed by the scanning head. The idea was to force the ejected material to accumulate on the side of the groove, which will be removed by the successive passes of the ablation process. In this way the external edge separating the ablated area from the sample surface could be protected from the material accretion generated by the localized pressure wave of the vaporized material evolving from the groove. ShFM measurements reported in Fig. 13 show that an even minimal inclination of the beam axis with respect to the specimen surface generated a remarkable slope of the groove profile.

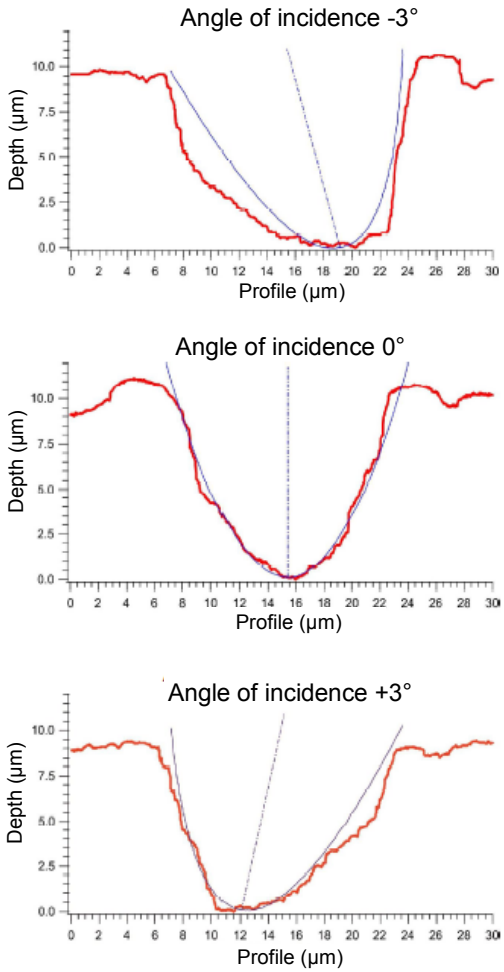

Fig.13. Groove profiles extracted from ShFM maps for: sample 19 AI=-3°; sample 2 AI=0°; sample 18 AI=3°. The precessional axis of the beam is located at the left side of the groove.

Concerning the groove bulges, when ablating perpendicularly to the surface (AI=0°) the material was found almost uniformly on both external (right) and internal (left) edges. Conversely, when an angle of incidence is applied the material tended to accumulate of the edge opposed to the inclination of the beam. Taking into account that the precessional axis of the beam is placed at the left side of the profiles in Fig. 13, using a positive angle of incidence (AI=+3°) could provide with a viable strategy in order to convey debris towards the centre of the circular area, where they are further ablated by the successive laser pulses. Using AI higher than 3° resulted in a distorted parabolic profile which limited the use of the empirical model developed in the previous sub-section due to a non homogeneous reflection of the laser radiation on the specimen surface.

3.4 Removal of layers

The beam was moved in spiral trajectories to perform the removal of circular layers, having external diameters of 300 μm and 600 μm. The trajectory started at a distance of 10 μm (corresponding to the laser spot radius) from the rotational axis. The radial overlap of the grooves or radial hatch distance was

varied by selecting the number of turns n_t needed to complete the spiral trajectory. The radial overlap RO can be then calculated as follows:

$$RO = \frac{\phi_{SPOT} \cdot n_t - r_{layer}}{n_t} \quad (8)$$

where r_{layer} is the radius of the layer to be removed. According to this definition, RO can assume negative values in case of negligible overlap, and large positive values when a strong overlap occurs.

Given the difficulty to obtain the removal of layers using the numerous combinations of process parameters reported in table 2, the approach followed for the removal of layers consisted in the adoption of a further parameter named rotational frequency f_{rot}. The rotational frequency represents the maximum number of turns obtainable in 1 s by the scanning head. The reciprocal of the rotational frequency is the minimum obtainable time to perform a turn (e.g. 0.01 s at 100 Hz): this characteristic time was kept constant during the ablation along the spiral trajectories meaning that the travelling speed of the beam, tangential to the trajectory, increases linearly with increasing the spiral radius according to $v = 2 \pi R f_{rot}$, with R the radius of the circular mark. By adopting this method it was possible to obtain, in the removal of a single layer, an entire range of energy density and to evaluate whether the ablated depth changed evenly with ED.

Table 3. Levels and values for selected parameters.

	Parameters			
Sample n°	Layer radius, r_{layer} (μm)	Pulse energy, E_P (μJ)	Rotational frequency, f_{rot} (Hz)	Number of turns, n_t
1	150	50	80	6,12,24,48,96
2	150	50	100	6,12,24,48,96
3	150	10	100	6,12,24,48,96
4	150	10	80	6,12,24,48,96
5	150	5	80	6,12,24,48,96
6	150	5	100	6,12,24,48,96
7	150	5	100	6,12,24,24,30
8	150	5	80	6,12,24,24,30
9	150	10	80	6,12,24,24,30
10	150	10	100	6,12,24,24,30
11	300	10	100	12,18,24,30,36
12	300	10	80	12,18,24,30,36
13	300	10	60	12,18,24,30,36
14	300	5	100	12,18,24,30,36
15	300	5	80	12,18,24,30,36
16	300	5	60	12,18,24,30,36
17	300	15	100	12,18,24,30,36
18	300	15	80	12,18,24,30,36
19	300	15	60	12,18,24,30,36

Noticeably, after a few preliminary tests (samples 1 and 2 of table 3) it was clear that using ED higher than a few J/mm^2 generated an irregular ablation process characterized by plasma and even melt ejection. Despite the ultrashort pulsed duration, the 100 kHz repetition rate combined to radial overlap of 1 to 10 μm resulted in a not negligible thermal transfer to the workpiece increasing drastically with the number of passes. As a result, to keep the ablative nature, which allowed a predictable and refined material removal of the process developed so far, the pulse energy was varied in the range of 5 to 15 μJ. The use of ED below 1 J/mm^2 also reduced the formation of burrs along channel edges, thus favouring the use of an incidence angle AI = 0°.

The ShFM analysis has been carried out on several samples machined with different choices of the following experimental parameters: laser pulse energy E_P, rotational frequency f_{rot}, number of turns n_t, the latter determining the radial overlap, or radial hatch distance, of contiguous engraved marks.

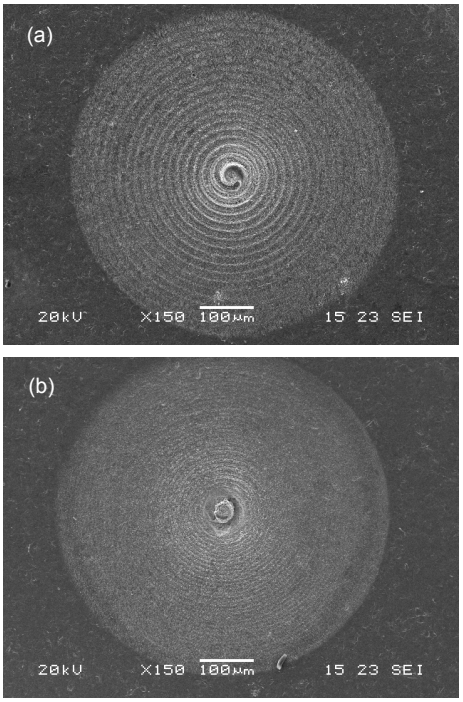

Fig.14. SEM images of two layers in sample 13 removed using E_P = 10 μJ, f_{rot} = 60 Hz and (a) n_t = 18; (b) n_t = 36.

As an example, Fig. 14 demonstrates in a top view the influence of doubling the number of passes on the uniformity of the surface. The increase of tangential speed when moving towards the external diameter generates a difference in the removed depth, whose effects are clearly visible if compared to the center of the layer.

The topography of the layer machined at E_P = 10 μJ, f_{rot} = 60 Hz, n_t = 18 on a r_{layer} = 300 μm total radius is reported in Fig. 15 (a). Due to the relatively small radial overlap attained RO = 3 μm (testified by the inter-mark distance, around 17 μm, which is in turn similar to the laser spot diameter ϕ_{SPOT}), individual grooves are clearly discerned. In particular, portions of seven distinct grooves are identified as dark traces in the map, corresponding to turns number 5–11 (counted from the border). Their radius lies in the approximate range $R \sim$ 200–100 μm. The cross-section analysis, carried out along the dashed segment superposed to the image and reported as a line profile in Fig. 15(b), shows an average groove depth around 1.2 μm. The energy density for the imaged grooves can be calculated using eq. (1), with $v = 2\pi R f_{rot}$, leading to $ED \sim$ 0.6–1.2 J/mm^2. The measured depth turns out in rough agreement with data reported in Fig. 6. As far as the width is concerned, the presence of neighbouring marks hampers a reliable evaluation of the theoretical plane, hence of the width according to the procedure described in Fig. 5.

The example considered in Fig. 15 enables highlighting two additional aspects, which have been found in the majority of the

scans performed on the samples. First of all, the average topographical level, or height, of the machined surface is slightly decreasing in function of the distance from the border of the spiral, as suggested by the line profile of Fig. 15 (b). In addition, the surface roughness depends also on that distance. In order to demonstrate this statement, the analyzed surface has been divided into square portions of individual size 20 µm x 20 µm, and the corresponding areal roughness S_a (the analogous of R_a for a surface) has been determined. As shown in Fig. 15 (c), the so-measured roughness tends to increase when moving from the border to the centre of the machined spiral.

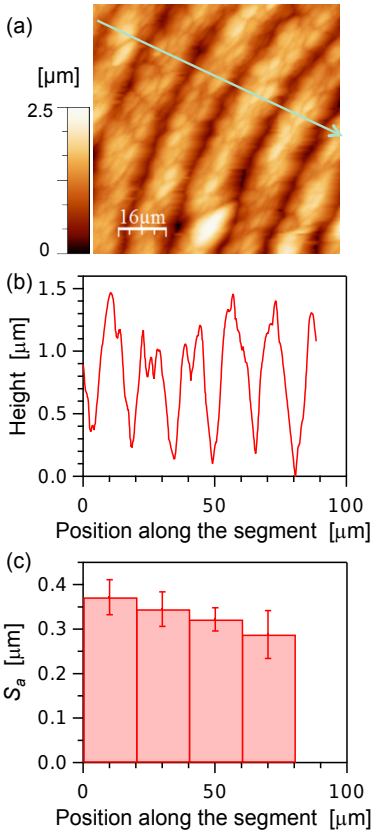

Fig. 15. Example of ShFM analysis on a sample machined at E_P = 10 µJ, f_{rot} = 60 Hz, n_t = 18 (sample 13). Panel (a) shows the topography map (the zero of the color scale corresponds to the minimum height in the image), panel (b) the line profile analysis carried out along the segment superposed to the topography map (the arrow indicates the direction pointing towards the centre of the spiral), panel (c) the areal roughness S_a measured on 20 µm x 20 µm square portions of the topography map. The error bars are evaluated on the basis of repeated measurements on different square portions.

Such aspects can be better illustrated by looking at large machined surfaces that cannot be accomplished in a single ShFM scan due to limitations in the maximum travel of the nanopositioner. Fig. 16 reports the result of a gluing process, where four subsequent scans on the same sample (machined at E_P = 5 µJ, f_{rep} = 100 Hz, n_t = 30 on a r_{layer} = 300 µm total radius), acquired by displacing the tip along one direction at the end of every scan, have been superposed each other in order to image the large part of the machined surface width and a small portion of the bare (non-machined) substrate. It can be noted that, the large energy density achieved in the marks close to the center, where the process starts, leads to very irregular surfaces preventing a reliable topography reconstruction. Therefore, the region close to the center of the spiral has been disregarded in the imaging; the overall size of the obtained map is 280 µm x 100 µm.

The topography map, fig. 16 (a), clearly demonstrates that for low *ED* values (in the first ten turns counted from the border the energy density, calculated as mentioned above, is $ED \leq 0.2$ J/mm^2) the engraved marks are hardly distinguishable from the surface roughness. As a consequence, individual grooves cannot be clearly discerned in the map. Conversely, at increasing *ED*, i.e., for marks closer to the centre of the spiral, grooves are identified, showing an increasing depth when approaching the spiral center.

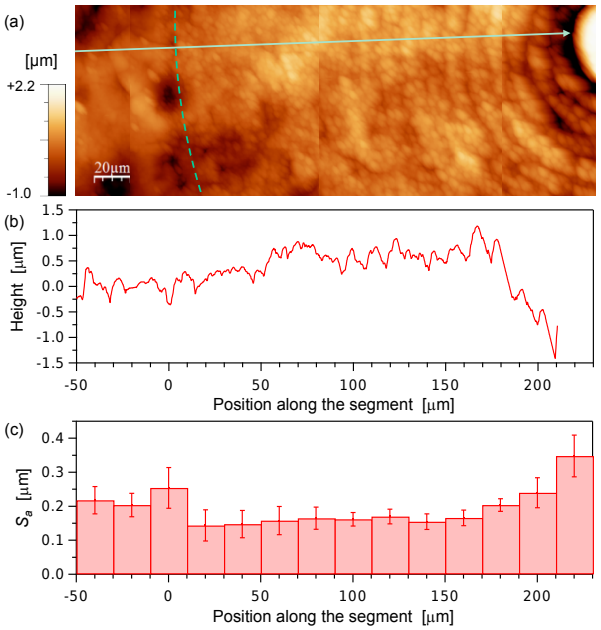

Fig. 16. Composition of four different ShFM scans on a sample machined at E_P = 5 µJ, f_{rot} = 100 Hz, n_t = 30 (sample 14). Panels (a)–(c) as in Fig. 15. Note that, in this case, the height is referenced to the average level of the non-machined part, determined here with an uncertainty of ± 63 nm. The dashed line in panel (a) represents the boundary between the non-machined and the machined portions of the surface (on the left and right, respectively), assumed as the zero for the horizontal axis in the plots of panels (b) and (c).

The colour scale of the map is, in this case, referenced to the average height of the non-machined region, carefully ascertained through repeated scans. Note that the uncertainty associated with such evaluation, which amounts to several tens of nanometres, is not included in the determination of the reference level. The same scans allowed us also to determine the areal roughness of the bare substrate, S_a = (204±32) nm, evaluated on several 20 µm x 20 µm square portions of the surface.

The line profile analysis reported in Fig. 16 (b) suggests that, when moving from the border to the centre of the spiral, there is initially an apparent small increase in the average height of the machined surface, possibly due to accumulation of burrs and re-deposited material. According to the results presented in section 3.3, inclining the beam by a small negative value of the incidence angle, might be a viable approach to reduce such an effect and improve the roughness. Approaching the centre of the spiral, where the energy density gets larger and larger, material removal prevails, leading to a marked decrease in the average height. In the example considered here, the transition to the decreasing trend occurs at a calculated $ED \sim 0.5$ J/mm^2. Evaluation of the finishing properties, determined as mentioned above and shown in Fig. 16 (c), demonstrates that the areal roughness S_a in the outer portions of the spiral is consistently smaller than for the bare substrate. Therefore, even though laser irradiation does not produce a measurable material removal and the consequent formation of individual grooves, it is effective in modifying the finishing properties. Close to the centre, S_a starts increasing,

essentially because of the presence of well-resolved and deep individual grooves.

By increasing the number of turns, that is the radial overlap, individual grooves are no longer discerned even for large *ED* values. As an example, Fig. 17 shows the topography map of a sample machined at E_P = 5 μJ, f_{rot} = 100 Hz, n_t = 96 on r_{layer} = 150 μm (*RO* = 18 μm). In this case, the distance between neighbouring marks, around 1.6 μm, is much smaller than the laser spot diameter ϕ_{SPOT} and the local topography is due to the convolved effect of multiple laser irradiation. The starting point of the scan, i.e., the left side of the imaged portion, is located around 30 μm from the border of the spiral. Considering the selected scan size of 80 μm x 80 μm, the centre of the map is hence placed at around 2/3 of the machined region length. The areal roughness, evaluated as described above, turns out S_a = (96±22) nm. Furthermore, the height of the map, measured at its centre, is found to be Δh = (1.2±0.2) μm below the average level of the non-machined surface, where the quoted uncertainty accounts for both the residual inclination of the scanned region and the errors in identifying the reference level. The spiral-like trajectory of the machining laser spot leads to effectively mill the sample surface, and Δh can be interpreted as the depth of cut, or thickness of the ablated layer, at the mentioned position.

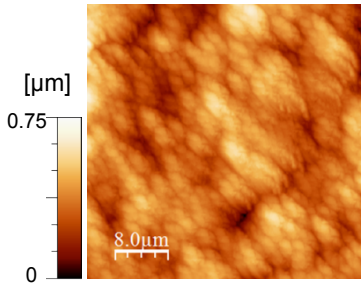

Fig. 17. Topography map of a sample machined at E_P = 5 μJ, f_{rep} = 100 Hz, n_t = 96 (sample 6); the zero of the colour scale corresponds to the minimum height in the image. The border of the spiral is located around 30 μm to the left of the image.

Both S_a and Δh depend on the machining parameters. In order to illustrate the observed trends, a set of ShFM scans carried out in conditions similar to those of Fig. 17 has been realized on different samples. For the sake of comparison, the starting point of the scans has been set for all samples as described above. The machining parameters have been characterized by using the energy density *ED* calculated in the centre of the map, i.e., assuming *R* = 100 μm, and the comparison has been restricted to surfaces where individual grooves cannot be clearly identified in the topography maps (i.e., for samples machined at n_t = 96 and n_t = 48).

Results are summarized in Fig. 18: although in the presence of relatively large error bars, it is possible to infer a trend for S_a and Δh, which both tend to increase with *ED*. In other words, by delivering a larger laser energy dose to the surface, a more efficient material removal is accomplished, even though the inferred dependence is strongly sub-linear. On the other hand, a larger energy dose produces less regular surfaces, as demonstrated by the slight increase in S_a. A role can also be deduced for n_t : when the spiral consists of strongly superposed grooves, a slightly more regular surface is achieved accompanied with a more efficient material removal.

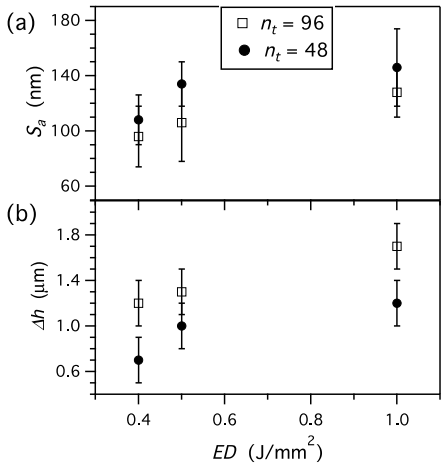

Fig. 18. Areal roughness S_a (a) and material removal Δh (b) as a function of the energy density *ED* (all quantities defined as in the text). Data are derived from the ShFM analysis of different samples machined at different parameters, including the number of turns n_t as specified in the legend (samples: 3, 4, 5).

4. Conclusions

A preliminary investigation that gives fundamentals to a novel laser micro-milling process was performed in the present study. The process makes use of an ultrashort pulsed laser moved in spiral trajectories generating a repeatable depth of cut over circular layers. The ablation of more complex 3D structures, which was not the focus of the present study, could be attained by imposing a feed motion to the specimen holder and propagating the ablation at a constant speed.

Even considering the complexity of the ablation strategy and the amount of variables playing a role in the removal of grooves and layers, the research allowed to obtain predictable depth of cut ranging between 0.6 to 1.8 μm with an areal roughness in the range of 100-150 nm. It was demonstrated that understanding the influence of process parameters on the morphology of grooves and circular layers allowed to solve the trade off between productivity and surface roughness that affects the majority of laser micro-milling processes based on the flanking of parallel grooves. Despite the extremely small material removal rate obtainable with an 800 fs pulsed laser at *ED* lower than 1 J/mm^2, which on the other hand favored extra-smooth surfaces, the process can find an industrial relevance when high number of turns are used to generate spiral trajectories. The selected repetition rate of 100 kHz combined with a tangential speed up to 75 mm/s, allowed for continuous removal along a single groove. The rotational frequency fixed the time needed to ablate over one turn and even with the highest number of turns, layers were removed in less than 1 s. The use of such a kind of laser source, under a limited regime of pulse energies, promoted a pure ablation process thus avoiding all those undesired phenomena related to heat transfer e.g. uneven roughness, unpredictable depth of cut. On the other hand modulating the number of turns can be used to prevent any observable track of the circular grooves on the machined surface and to increase its uniformity and isotropy.

The micro-milling of step-like structures to be obtained by the removal of multiple superimposed layers is obviously out of the scope of the present paper. Nonetheless, accuracy and surface roughness obtained after the preliminary investigations of the present research, open the way for devising strategies able to obtain step-like micro-structures with refined surface flatness and uniformity.

References

[1] Mishra S, Yadava V. Laser Beam Micro Machining (LBMM) - A review. Optics and Lasers in Engineering 2015; 73: 89-122.

[2] Viboon Tangwarodomnukun. Cavity formation and surface modeling of laser milling process under a thin-flowing water layer. Applied Surface Science. 2016; 386, 1: 51-64.

[3] Wang W, Chen J, Li D, Feng D, Tu Y. Modelling and optimisation of a femtosecond laser micro-machining process for micro-hole array products. International Journal of Advanced Manufacturing Technology 2016; 82: 1293-1303.

[4] Saklakoglou IE, Kasman S. Investigation of micro-milling process parameters for surface roughness and milling depth. International Journal of Advanced Manufacturing Technology 2011;54:567–78.

[5] Teixidor D, Ferrer I, Joaquim Ciurana J, Özel T. Optimization of process parameters for pulsed laser milling of micro-channels on AISI H13 tool steel. Robotics and Computer-Integrated Manufacturing 2013; 29: 209–218.

[6] Campanelli SL, Casalino G, Contuzzi N. Multi-objective optimization of laser milling of 5754 aluminum alloy. Optics & Laser Technology 2013; 52: 48-56.

[7] Meijer J, Du K, Gillner A, Hoffmann D, Kovalenko VS, Masuzawa T et al. Laser machining by short and ultrashort pulses, state of the art and new opportunities in the age of photons. CIRP-Annals – Manufacturing technology 2002; 51 (2) : 531-550.

[8] Leitz KH, Redlingshöfer B, Reg Y, Otto A, Schmidt M. Metal ablation with short and ultrashort laser pulses. Physics Procedia 2011;12:230–8.

[9] Yao YL, Chen HL, Zhang W. Time scale effects in laser material removal: a review. International Journal of Advanced Manufacturing Technology 2005 ; 26 (5): 598–608

[10] Cheng J, Perrie W, Edwardson SP, Fearon E, Dearden G, Watkins KG. Effects of laser operating parameters on metals micromachining with ultrafast lasers. Applied Surface Science 2009; 256: 1514–1520.

[11] Zhou W, Ling WS, Liu W, Peng Y, Peng J. Laser direct micromilling of copper-based bioelectrode with surface microstructure array. 2015 Optics and Lasers in Engineering 2015; 73: 7-15.

[12] Romoli L, Tantussi G, Dini G. Layered Laser Vaporization of PMMA Manufacturing 3D Mould Cavities. Annals of the CIRP 2007; 56(1): 209-212.

[13] Genna S, Leone C, Lopresto V, Tagliaferri V. An experimental study on the surface mechanisms formation during the laser milling of PMMA. Polymer Composites 2015; 36 (6): 1063-1071.

[14] Kibria G, Doloi B, Bhattacharyya B. Investigation into the effect of overlap factors and process parameters on surface roughness and machined depth during micro-turning process with Nd:YAG laser. Optics & Laser Technology 2014; 60:90–98.

[15] Bartolo P, Vasco J, Silva B, Galo C. Laser micromachining for mould manufacturing: I. The influence of operating parameters. Assembly Automation 2006; 26(3):227–234.

[16] Eberle G, Dold C, Wegener K. Picosecond laser fabrication of micro cutting tool geometries on polycrystalline diamond composites using a high-numerical aperture micro scanning system. Proceedings of SPIE - The International Society for Optical Engineering 9351, 935104.

[17] Shih-Feng Tseng, Ming-Fei Chen, Wen-Tse Hsiao, Chien-Yao Huang, Chung-Heng Yang, Yu-Sheng Chen. Laser micromilling of convex microfluidic channels onto glassy carbon for glass molding dies. Optics and Lasers in Engineering 2014; 57: 58–63.

[18] http://www.arges.de/industrial-products/precession/

[19] Tantussi F, Vella D, Allegrini M, Fuso F, Romoli L, Rashed CAA Shear-force microscopy investigation of roughness and shape of micro-fabricated holes. Precision Engineering 2015; 41: 32-39.

[20] Ordal MA, Bell RJ, Alexander Jr RW, Long LL, Querry MR (1985) Optical Properties of Fourteen Metals in the Infrared and Far Infrared. Applied Optics 24:4493–4499.

- ✓ Micromilling of stainless steel is performed with a fs-pulsed laser
- ✓ Layers are ablated moving the beam along spiral trajectories
- ✓ The profile of a single groove is related to process parameters
- ✓ The depth of cut per layer is studied as a function of process parameters.
- ✓ Areal roughness Sa lower than 100 nm can be attained on the ablated surface